Yeast Num1p Associates with the Mother Cell Cortex during S/G2 Phase and Affects Microtubular Functions

Marian Farkasovsky and Hans Küntzel

Max-Planck-Institut für experimentelle Medizin, D-37075 Göttingen, Federal Republic of Germany

Abstract. The *NUM1* gene is involved in the control of nuclear migration in *Saccharomyces cerevisiae*. The content of *NUM1* mRNA fluctuates during the cell cycle, reaching a maximum at S/G2 phase, and the translation product Num1p associates with the cortex of mother cells mainly during S, G2, and mitosis, as seen by indirect immunofluorescence. The nuclear spindle in *NUM1*-deficient large-budded cells often fails to align along the mother/bud axis, while abnormally elongated astral microtubules emanate from both spindle pole bodies. A *num1* null mutation confers temperature sensitivity to the cold-sensitive α-tubulin mutant *tub1-1*, and shows synthetic lethality with the β-tubulin mutant alleles *tub2-402, tub2-403, tub2-404,* and *tub2-405*. Deletion mapping has defined three functionally important Num1p regions: a potential EF hand Ca^{2+} binding site, a cluster of potential phosphorylation sites and a pleckstrin homology domain. The latter domain appears to be involved in targeting Num1p to the mother cell cortex. Our data suggest that the periodically expressed *NUM1* gene product controls nuclear migration by affecting astral microtubule functions.

THE proper distribution of segregated chromosomes between mother and daughter cells requires the migration of the nucleus to the bud neck and the positioning of the pre-anaphase spindle along the mother/bud axis during the G2 phase of the yeast cell cycle (Byers and Goetsch, 1975; Pringle and Hartwell, 1981). Nuclear migration and positioning critically depends on the functions of astral microtubules (AMTs)[1] emanating from the cytosolic side of the two spindle pole bodies (SPBs) (Palmer et al., 1992), as manifested by the effects of microtubule inhibitors (Jacobs et al., 1988) and by the phenotypic properties of β-tubulin (*tub2*) mutants (Huffaker et al., 1988; Palmer et al., 1992). Furthermore, the nuclear migration defects of actin mutants suggest that actin may play a role in tethering astral microtubules to the cytoskeleton during the migration process (Palmer et al., 1992). The asymmetric segregation of the old and new SPB between mother and daughter cell, respectively (Vallen et al., 1992), suggests a specific functional orientation of SPBs toward the cortex of mother and bud compartment at G2, presumably mediated by AMTs.

At least four additional genes (*DHC1/DYN1, JNM1, ACT3/ACT5* and *NUM1*) are involved in nuclear migration control, since strains lacking one of these nonessential genes accumulate cells with misoriented nuclei dividing in the mother compartment. *DHC1/DYN1* encodes the heavy chain of the dynein motor complex which is probably involved in pulling the bud-proximal astral microtubules into the bud (Li et al., 1993; Eshel et al., 1993), whereas *JNM1* appears to encode an accessory dynein protein involved in tethering astral microtubules to the bud cytoskeleton (McMillan and Tatchell, 1994). The actin/Arp1-related *ACT3/ACT5* protein is a homolog of human α-centractin and a major component of a dynactin complex believed to support the dynein motor activity (Muhua et al., 1994; Clark and Meyer, 1994).

The *NUM1* gene (Kormanec et al., 1991) encodes a 313-kD protein containing twelve near-identical tandem repeats of a peptide of 64 residues; the repeat unit itself is composed of two proline-punctuated homologous 32-amino acid peptides each containing two α-helical regions. The amino-terminal region exhibits a coiled-coil (heptad repeat) domain (Lupas et al., 1991) followed by a potential EF hand Ca^{2+}-binding site, and a pleckstrin homology (PH) domain was recently detected at a carboxy-terminal region of Num1p (Gibson et al., 1994).

The deletion of the *NUM1* gene does not affect viability, but causes the accumulation of large-budded cells with two DAPI-stained chromosomal regions in the mother compartment. Furthermore, *NUM1*-deficient cells tend to diploidize during mitosis, and homozygous *num1* diploids form multispored asci upon sporulation (Kormanec et al.,

1. *Abbreviations used in this paper:* AMT, astral microtubule; GST, glutathione-*S*-transferase; MM, selective minimal medium; PH, pleckstrin homology; SPB, spindle pole body; YPD, rich medium.

1991). More recently, a polymorphism of the repetitive region of *NUM1* (allelic with *RVS272*) was reported in various strains, with repeat numbers varying between 1 and 24; furthermore, the percentage of binucleated large-budded mother cells in *rvs272* or *num1* populations was found to increase after entering stationary phase (Revardel and Aigle, 1993).

In this study we report the cell cycle–specific expression and cellular localization of the *NUM1* gene product, the effects of *NUM1* deletions on microtubule morphology and nuclear positioning, and genetic interactions with tubulin mutants. We further report evidence that the carboxy-terminal PH domain is required to target Num1p to the mother cortex. Our observations suggest that Num1p controls the proper alignment of the nuclear spindle along the mother/bud axis by affecting microtubule functions.

Materials and Methods

Reagents

β-Glucuronidase/Arylsulfatase, 4′,6′-diamino-2-phenylindole (DAPI) and restriction endonucleases were purchased from Boehringer (Mannheim FRG). Monoclonal anti-chicken brain α-tubulin, FITC-labeled goat anti–rabbit IgG and FITC-labeled rabbit anti–goat IgG were purchased from Sigma Chemical Co. (St. Louis, MO). Rhodamine-conjugated phalloidin was purchased from Molecular Probes, Inc. (Eugene, OR). Glutathione-Sepharose and protein A–Sepharose were purchased from Pharmacia LKB (GmbH, Freiburg, FRG). Plasmids and *E. coli* strains were purchased from Stratagene GmbH (Heidelberg, FRG). Reagents for DNA purification, RNA, and protein purification were purchased from Sigma and from Qiagen GmbH (Hilden, FRG). Restriction enzymes, ligases, and nucleases were purchased from New England BioLabs (GmbH, Schwalbach, FRG). α pheromone was a kind gift of W. Schmidt.

Plasmid Constructions

Fig. 1 shows the restriction map of the genomic *KGD2-NUM1* region, indicating sites of deletions and subcloned regions of the *NUM1* gene. The *NUM1* flanking and coding region was subcloned in pUC19 as an upstream 4.4-kb SalI–XbaI fragment (pJK23), a central 4.3-kb XbaI fragment (pJK24), and a downstream 8.4-kb HindIII fragment (pJK27) (Kormanec et al., 1991). pJK28 was obtained by introducing a 1.6-kb YEp24/HindIII(repaired) fragment containing the *URA3* gene into the XbaI(repaired) site of pUC19.

Plasmid pFM18 contains the entire *NUM1* flanking and coding region in the *CEN6/ARSH4/HIS3* vector pRS313. Construction steps: a 4.3-kb pJK24–XbaI fragment was inserted into XbaI-linearized pJK23 to obtain pFM10; a 5.2-kb pFM10/PstI fragment was inserted into PstI-linearized pEMBL19 to obtain pFM13; a 5.1-kb pJK27/BstEII fragment was inserted into BstEII-linearized pFM13 to obtain pFM15; a 10-kb pFM15/BamHI fragment (using a vector-derived BamHI site) was inserted into pRS313 to obtain pFM18.

Plasmid pFM70 (*num1-Δ1::URA3*) was obtained by inserting an end-repaired 1.6-kb YEP24/HindIII *URA3* fragment between the flanking SpeI sites of pFM18. Alternatively, the same *URA3* fragment was inserted between AsuII and SpeI sites of pFM18, followed by the insertion of a 1-kb SacI fragment containing the *NUM1* 3′ end into the single SacI site, to obtain pFM75 (*num1-Δ2::URA3*). The two *num1::URA3* alleles were introduced into yeast as BstEII–HindIII fragments of pFM70 and pFM75, respectively.

Construction of pFM19 (*num1-Δ3*): a 4.3-kb pJK24/XbaI fragment was inserted into XbaI-linearized pBluescript II KS to obtain pFM4; a 1.2-kb BamHI–SalI fragment of pJK28 (using vector-derived sites) was placed between the respective sites of pFM4 to obtain pFM6; pFM7 was obtained by EcoRI digestion/religation of pFM6, deleting 11 out of 12 repeats; a 1.8-kb pFM7/XbaI fragment was inserted into the XbaI site of pJK23 to obtain pFM11; a 3.5-kb pFM11/BamHI fragment (using one vector-derived BamHI site) was inserted into the BamHI site of pUC19 to obtain pFM12; a 5.1-kb pJK27/BstEII fragment was inserted into the BstEII site of pFM12
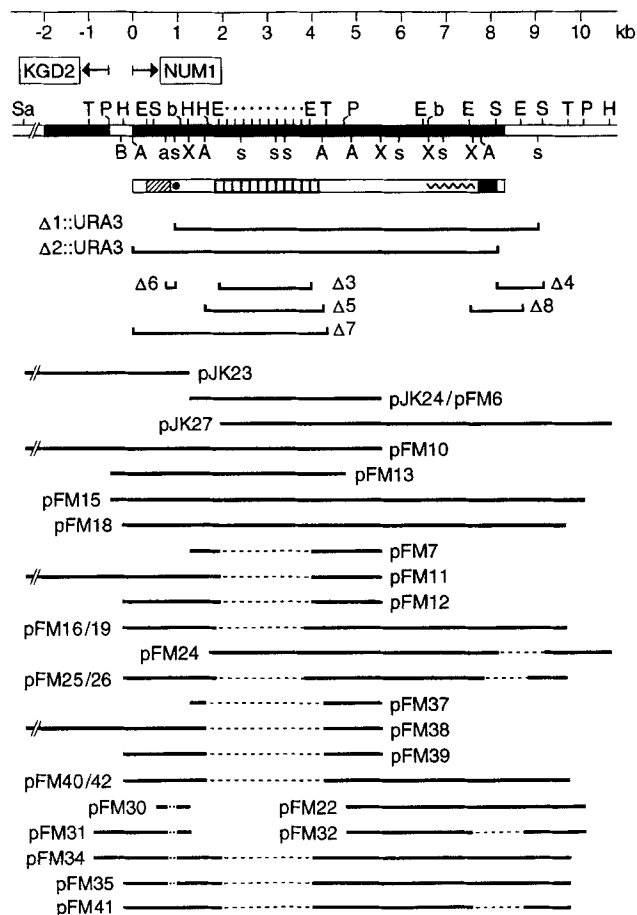

Figure 1. Restriction map of *NUM1* clones. (*Upper part*) Map of the divergently transcribed *KGD2-NUM1* chromosomal region. (*Black boxes*) Coding regions; (*open boxes*) noncoding regions. Restriction sites: A, AsuII; a, AseI; B, BamHI; b, BglII; T, BstEII; E, EcoRI; P, PstI; S, SacI; Sa, SalI; s, SpeI; X, XbaI. A cluster of 12 regularly spaced EcoRI sites is indicated by dots. The protein map of the *NUM1* coding region shows the following features: (*shaded box*) coiled-coil (heptad repeat) domain; (*black dot*) a potential EF hand Ca^{2+}-binding site; (*heavy boxes*) 12 near-perfect tandem repeats; (*waved line*) epitope recognized by polyclonal antibodies; (*black box*) PH domain. *NUM1* regions deleted in alleles *num1-Δ1* to *num1-Δ8* and *NUM1* subclones (plasmid inserts) are shown in the middle and lower part, respectively. Deletions of subcloned regions are indicated by dotted lines.

to obtain pFM16; a 8.8-kb pFM16/BamHI fragment was introduced into the BamHI site of the centromeric plasmid pRSR313 to obtain pFM19.

Construction of pFM26 (*num1-Δ3,Δ4*): a 1-kb SacI fragment was deleted from pJK27 to obtain pFM24; a 4.1-kb pFM24/BstEII fragment was inserted into the BstEII site of pFM12 to obtain pFM25; a 7.8-kb pFM25/BamHI fragment (using one vector-derived site) was inserted into pRSR313 to obtain pFM26.

Construction of pFM42 (*num1-Δ5*): pJK24 was partially digested with AsuII and religated to obtain pFM37 (deletion of all 12 repeats); a 1.7-kb pFM37/XbaI fragment was inserted into the XbaI site of pJK23 to obtain pFM38; a 3.3-kb pFM38/BamHI fragment (using a vector-derived BamHI site) was inserted into the BamHI site of pUC19 to obtain pFM39; a 5.1-kb pJK27/BstEII fragment was inserted into the BstEII site of pFM39 to obtain pFM40; an 8.5-kb pFM40/BamHI fragment (using a vector-derived site) was inserted into pRSR313 to obtain pFM42.

Construction of pFM35 (*num1-Δ3,Δ6*): a 0.8-kb SacI–HindIII fragment of pFM12 was inserted between the respective sites of pUC19 to obtain

pFM29; a 5'-TAGCTTAG-3' linker was placed between a AseI (partial digestion) and SpeI sites of pFM29 to obtain pFM30; a 1.4-kb BstEII(repaired)/SacI fragment of pJK23 was introduced between the pUC19-derived repaired EcoRI site and the insert SacI site of pFM30 to obtain pFM31; a 6.4-kb BglII–SalI pFM16 fragment (flanked by the NUM1 downstream BglII site and a vector-derived end-repaired SalI site) was inserted between the single BglII site and the downstream end-repaired HindIII site of pFM31 to obtain pFM34; an 8-kb pFM34/BamHI fragment (using one vector-derived site) was inserted into the BamHI site of pRS313 to obtain pFM35.

Construction of pFM52 (num1-Δ7): a 5.1-kb pFM15/BstEII fragment was inserted into a derivative of the two-hybrid vector pGBT9 (Clontech, Palo Alto, CA) containing a single BstEII site in the fusion site, to obtain pFM52; this plasmid encodes the DNA-binding domain of the GAL4 protein fused to the COOH-terminal half of Num1p.

Construction of pFM41 (num1-Δ3,Δ8): a 5.4-kb pJK27/PstI fragment was inserted into the PstI site of a pUC19 derivative lacking a EcoRI site, to obtain pFM22; a 1-kb pFM22/EcoRI fragment was inserted into EcoRI-linearized pFM22 to obtain pFM32; a 4.4-kb pFM32/PstI fragment was inserted into the PstI site of pFM16 to obtain pFM36; a 4.4-kb pFM36/BstEII fragment was inserted between the two BstEII sites of pFM19 to obtain pFM41.

A 1-kb pJK27/EcoRI NUM1 fragment encoding residues 2182-2519 (Kormanec et al., 1991) was introduced into EcoRI-linearized pGEX-3X to obtain the glutathione-S-transferase (GST) fusion plasmid pFM71.

Yeast Strains and Media

The genotypes and origins of Saccharomyces cerevisiae strains used in this study are shown in Table I. Yeast strains were grown in YPD medium (1% bacto-yeast extract, 2% bacto-peptone, 2% glucose). Selective minimal media contained 0.67% yeast nitrogen base, 2% glucose and auxotrophic requirements. Solid media contained 2% agar. Diploid strains were allowed to sporulate on SP2 plates (1% potassium acetate, 2% agar). NUM1/URA3 gene exchange was performed by one-step gene replacement (Rothstein, 1983) and controlled by Southern hybridization of genomic DNA (Sambrook et al., 1989). Phenotypical properties of null mutant strains containing the alleles num1-Δ1::URA3 and num1-Δ2::URA3 (see Fig. 1) were found to be identical, and all observed lesions could be rescued by introducing the NUM1 plasmid pFM18, indicating that no other gene function was affected by the replacement procedure.

Bacterial Expression and Purification of a GST-Num1p Fusion Protein

The method of Smith and Johnson (1988) was used for induction and purification of fusion protein. The GST-Num1p fusion plasmid pFM71 was introduced into E. coli SURE competent cells (Stratagene, La Jolla, CA), and the resulting transformant was grown in M9 medium at 37°C to OD (600 nm) = 0.5 before adding isopropyl-β-thiogalactopyranosid to 1 mM. Cells were grown for another 2.5 h at 37°C and homogenized by sonication in PBS containing 1% Triton X-100. The fusion protein was purified by affinity chromatography on glutathione Sepharose.

Preparation of Antibodies

100 μg of affinity-purified GST-Num1p fusion protein was emulsified with Freund's complete adjuvant and injected subcutaneously in several places of the back of rabbits. After 14 and 45 d rabbits were boosted after the same procedure, except that incomplete adjuvant was used. Blood was collected 14 d after the last injection, and preimmune serum was collected three weeks before the initial injection. The IgG fractions were obtained by chromatography on protein A–Sepharose. Antibodies against GST were removed by incubation of IgG with GST immobilized on nitrocellulose strips, and anti-Num1p antibodies were affinity-purified on immobilized GST-Num1p fusion protein essentially as described (Smith and Fisher, 1984). To test the immunological specificity of antibodies, proteins of a crude yeast lysate were separated by SDS-PAGE using 5% polyacrylamide and blotted to nitrocellulose membranes for 20 h at 4°C and 8V/cm (Burnette, 1981). The blots were treated with TBST (0.15 M NaCl, 50 mM Tris-HCl, pH 7.2, 0.1% Tween 20) containing 5% nonfat milk for 2 h at room temperature, and incubated for 1 h at room temperature with 1:200 diluted affinity-purified anti-Num1p antibodies in the same buffer. Immunodetection was accomplished by using biotinylated anti–rabbit antibodies and streptavidin-biotinylated horseradish peroxidase complex with the enhanced chemiluminescence Western blotting detection system (ECL, Amersham).

Immunofluorescence Microscopy

A modification of published protocols (Kilmartin and Adams, 1984; Pringle et al., 1991) was used. Asynchronously growing cultures of the NUM1 wild-type strain HK1b or synchronized cultures of the bar1 strain RH270-

Table I. Yeast Strains Used in This Study

Strain	Genotype	Source
HK1b	MATα ura 3-52 his3-Δ200	a
DBY1828	MATa ura3-52 his3-Δ200 trp1-1 leu2-3, 112 ade2	b
DBY1829	MATa ura3-52 his3-Δ200 trp1-1 leu2-3, 112 lys2-801	b
FMY1	MATa ura3-52 his3-Δ200 trp1-1 leu2-3, 112 ade2 num1-Δ1::URA3	c
FMY2	MATα ura3-52 his3-Δ200 trp1-1 leu2-3, 112 lys2-801 num1-Δ1::URA3	c
RH270-2B	MATa ura3-52 leu2-3, 112 his4-539 lys2-801 bar1	d
CC15	MATa ura3-52 his3-Δ200 ade2-101 cdc15-2	e
DBY2499	MATa ura3-52 his4-539 lys2-801 tub1-1	f
DBY2500	MATα ura3-52 ade2-101 tub1-1	f
FMY60	DBY2499 × DBY2500	c
FMY61	MATa/MATα ura3-52/ura3-52 his4-539/+ lys2-801/+ade2-101/+ tub1-1/tub1-1 num1-Δ1::URA3/+	c
HKY80	DBY2499 × FMY1	c
HKY80-2B	MATα ura3-52 his3-Δ200 trp1-1 leu2-3, 112 ade2-101 tub1-1 num1-Δ1::URA	c
TH133	MATa/MATα ura3-52/ura3-52 his4-539/+ ade2-101/+ tub2-104/tub2-104	g
TH134	MATa/MATα ura3-52/ura3-52 lys2-801/+ his4-539/+ ade2-101/+ tub2-401/tub2-401	g
TH135	MATa/MATα ura3-52/ura3-52 lys2-801/+ his4-539/+ ade2-101/+ tub2-402/tub2-402	g
TH136	MATa/MATα ura3-52/ura3-52 lys2-801/lys2-801 his4-539/+ ade2-101/+ tub2-403/tub2-403	g
TH137	MATa/MATα ura3-52/ura3-52 lys2-801/lys2-801 his4-539/+ ade2-101/+ tub2-404/tub-404	g
TH138	MATa/MATα ura3-52/ura3-52 lys2-801/+ his4-539/+ ade2-101/+ tub2-405/tub2-405	g
FMY13	MATa/MATα ura3-52/ura3-52 his4-539/+ ade2-101/+ tub2-104/tub2-104 num1-Δ1::URA3/NUM1	c
FMY14	MATa/MATα ura3-52/ura3-52 lys2-801/+ his4-539/+ ade2-101/+ tub2-401/tub2-401 num1-Δ1:: URA3/NUM1	c
FMY15	MATa/MATα ura3-52/ura3-52 lys2-801/+ his4-539/+ ade2-101/+ tub2-402/tub2-402 num1-Δ1::URA3/NUM1	c
FMY16	MATa/MATα ura3-52/ura3-52 lys2-801/lys2-801 his4-539/+ ade2-101/+ tub2-403/tub2-403 num1-Δ1::URA3/NUM1	c
FMY17	MATa/MATα ura3-52/ura3-52 lys2-801/lys2-801 his4-539/+ ade2-101/+ tub2-404/tub2-404 num1-Δ1::URA3/NUM1	c
FMY18	MATa/MATα ura3-52/ura3-52 lys2-801/+ his4-539/+ ade2-101/+ tub2-405/tub2-405 num1-Δ1::URA3/NUM1	c

a, Munder et al., 1988; b, Schatz et al., 1986; c, this study; d, obtained from H. Riezmann; e, Zwerschke et al., 1994; f, Stearns and Botstein, 1988; g, Huffaker et al., 1988.

2B were treated with 0.025% glutaraldehyde (added directly to the growth medium) for 5 min, followed by the fixation with 3.7% formaldehyde in PBS. After 60 min incubation at room temperature cells were washed 3× with PBS and suspended in 1 ml of solution A (1.2 M sorbitol, 50 mM Tris-HCl, pH 7.5, 0.5 mM MgCl₂, 10 mM 2-mercaptoethanol) containing 5 μl glucuronidase and 10 μl of a 30-mg/ml Zymolase solution. After 90 min incubation at 30°C cells were recovered by low speed centrifugation, washed twice with solution A, and incubated for 5 min at room temperature with 1% Triton X-100 in PBS. Cells were then washed with PBS containing 1% bovine serum albumin and allowed to settle for 3 min on poly-lysine-treated slides, which were subsequently air-dried and incubated for 30 min with a blocking solution (PBS containing 4% BSA and 1% nonfat dry milk). All subsequent incubations with antibodies were carried out in blocking solution at room temperature (or at 4°C if incubated overnight). Anti-Num1p and FITC-labeled antibody solutions were preabsorbed with num1 cells (strain FMY2).

The first incubation was with a 1:50 diluted solution of affinity-purified and preabsorbed anti-Num1p for 3 × 1 h, followed by an overnight incubation. The second incubation was with 3 μg/ml FITC-labeled goat anti-rabbit IgG for 2 × 1 h. The third incubation was with 6 μg/ml FITC-labeled rabbit anti-goat IgG for 2 × 1 h, followed by incubation with 1.5 μg/ml FITC-labeled goat anti-rabbit IgG for 2 × 1 h.

To costain Num1p, actin, and chromosomal DNA, slides were washed after the final antibody treatment with PBS and incubated with a 1-μM solution of rhodamine-conjugated phalloidin in PBS for 2 h. In a last step, cells were treated with 0.02 μg/ml DAPI, which was added directly to the mounting solution (PBS containing 90% glycerol and 1 mg/ml p-phen-ylenediamine). Costaining of microtubules and chromosomal DNA was performed by incubating slides (prepared as described above) with a 1:200 diluted solution of monoclonal anti-chicken brain α tubulin for 3 × 1 h. Slides were then washed with PBS and incubated with 1:40 diluted FITC-labeled rabbit anti-mouse IgG for 2 × 1 h. After washing, slides were mounted with a DAPI-containing mounting solution as described above. Cells were photographed on Kodak T-MAX 3200p using a Zeiss Ax-ioskop equipped for epifluorescence microscopy.

Results

Immunolocalization of Num1p

Polyclonal antibodies were raised against a carboxy-terminal peptide (residues 2182-2519) of Num1p, which was expressed in E. coli as a glutathione-S-transferase (GST) fusion protein and purified by glutathione-Sepharose affinity chromatography. Western blot analysis of crude lysate proteins has detected a major immunoreactive species corresponding in size to the 310-kD Num1 protein, as shown in Fig. 2 A. This band is undetectable in lysates of the NUM1-deficient strain FMY1 (lane B), but reappears if the NUM1 plasmid pFM18 is introduced into FMY1 (lane C). The 240-kD species seen in lane D corresponds in size to the num1-Δ3 product of plasmid pFM19. Preimmune serum did not produce a signal.

For localizing Num1p in intact cells, we have amplified the immunofluorescence signals by using three layers of FITC-labeled secondary antibodies. Row A of Fig. 3 shows exponentially grown NUM1 cells (strain HK1b) treated with anti-Num1p (left column) or DAPI (middle column) to stain Num1p and nuclei, respectively. All four cells visualized by phase contrast microscopy (right column) contain a single chromosomal region corresponding to G1, S, or G2 nuclei, and at least three cells are budded. The anti-Num1p fluorescence pattern indicates a dot-like distribution of Num1p concentrated at the cortex of cells, and in all budded cells the fluorescing material is found almost exclusively in the mother compartment. NUM1 cells treated with preimmune serum (row B) and num1-Δ1::URA3 cells (strain FMY2) treated with anti-Num1p (row C) do not
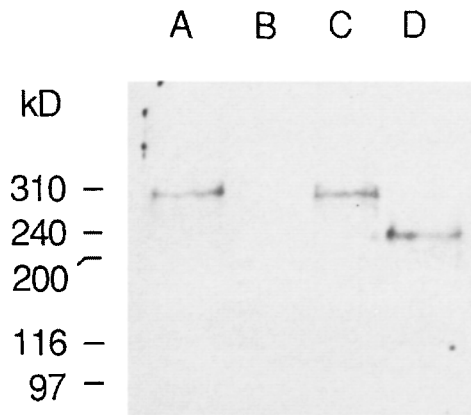

Figure 2. Western blot analysis of crude lysate proteins using anti-Num1p antibodies. (Lane A) Strain DBY1828 (relevant genotype NUM1); (lane B) strain FMY1 (num1-Δ1); (lane C) strain FMY1 containing plasmid pFM18 (num1-Δ1 NUM1); (lane D) strain FMY1 containing plasmid pFM19 (num1-Δ1 num1-Δ3). Size standards: rabbit myosin (200 kD), E. coli β-galactosidase (116 kD), and rabbit phosphorylase B (97.4 kD).

contain fluorescing material, supporting the specificity of the antibodies. DAPI staining of two budded NUM1-deficient cells (row C, second column) reveals the presence of two chromosomal spots in the mother compartment, a characteristic property of these mutants (Kormanec et al., 1991; Revardel and Aigle, 1993).

Periodic Fluctuation of NUM1 mRNA

Two observations prompted us to test a possible periodicity of NUM1 transcription and translation during the mitotic cell cycle: the NUM1 deletion affects the stage-specific process of nuclear migration (Kormanec et al., 1991), and Num1p specifically localizes to mother cells (see Fig. 3).

A pheromone-hypersensitive bar1,NUM1 strain was synchronized by release from pheromone arrest, and aliquots were removed at 15-min intervals for cytological determinations (budding state, spindle morphology) and for the isolation of total RNA. A mixture of two radiolabeled DNA probes (a 740-bp EcoRI–BglII NUM1 fragment and a 1.6-kb HindIII fragment containing the URA3 gene) was used to determine the levels of the 8.5-kb NUM1 mRNA together with the constitutively made 1-kb URA3 mRNA by Northern hybridization. As an additional control we have also measured CDC6 and CLN1 mRNAs, which accumulate at late mitosis and G1 (START), respectively (Zwerschke et al., 1994; Küntzel et al., 1994).

Fig. 4 demonstrates that the NUM1 mRNA content of pheromone-arrested cells (zero time) decreases to a minimum during the "return to the cycle" period at 15 min after release, and then reappears at a stage (45 min) where bud formation is initiated, while the nuclear spindle has not yet elongated. NUM1 mRNA drops to a low level during late mitosis and G1 phase (between 90 and 120 min) and reappears again at the onset of bud formation (135 min). Since bud initiation is a cytological marker associated with late S phase (Pringle and Hartwell, 1981), we conclude that NUM1 mRNA is induced at S phase and accumulates during S/G2. In contrast, CLN1 and CDC6 transcripts are not detected in pheromone-arrested cells
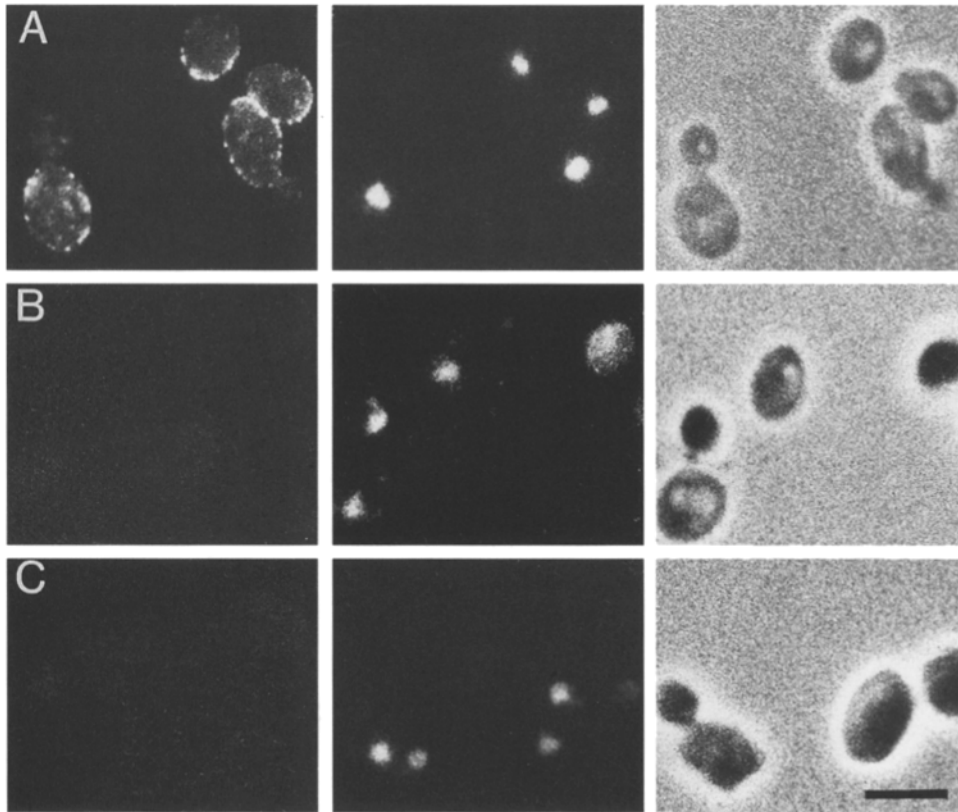
Figure 3. Subcellular localization of Num1p by indirect immunofluorescence microscopy (*first column from left*). Nuclear regions were stained with DAPI (*second column*), and cells were visualized by phase contrast microscopy (*third column*). (Row *A*) Strain HK1b (*NUM1*) treated with anti-Num1p antibodies. (Row *B*) Strain HK1b treated with preimmune serum. (Row *C*) Strain FMY2 (*num1-Δ1:: URA3*) treated with anti-Num1p antibodies. Bar, 10 μm.

and reappear already at 15 min after release. The second maximum of *CDC6* mRNA is formed at the telophase stage (elongated spindle) at 90 min, followed by the second *CLN1* mRNA maximum between the collapse of the mitotic spindle and bud initiation (around 120 min).

We consistently found that the level of *NUM1* mRNA starts to decrease already ~15 min after its appearance during the second cell cycle (between 135 and 150 min), although this second wave of expression should be extended, rather than shortened, due to a progressive loss of synchrony. This apparent discrepancy can be explained, however, by a marked instability of *NUM1* mRNA in cells grown under limiting nutrient supply (Kormanec, J., and H. Küntzel, unpublished observations), and the second *NUM1* transcription period in pheromone-synchronized cells is indeed extended if the culture is diluted into fresh medium at 120 min after release (data not shown).

We have also used an alternative method of cell cycle synchronization, the release of *cdc15-2* cells from telophase arrest (Zwerschke et al., 1994), to confirm the *NUM1* mRNA fluctuation pattern. As observed in pheromone-synchronized *bar1* cells, the maxima of the three transcripts (*CDC6*, *CLN1*, and *NUM1*) followed in this order in intervals of 15–20 min, and the *NUM1* mRNA maximum coincided with the onset of bud formation (data not shown).

Periodic Fluctuation of Num1p

Fig. 5 shows cells representative of populations removed from a pheromone-synchronized culture of the *bar1*, *NUM1* strain RH-270-2B at indicated times (*A–F*, see Fig. 4). Cells

were subsequently treated with anti-Num1p, rhodamine-conjugated phalloidin, and DAPI to visualize Num1p (*first column from left*), cortical actin dots (*second column*), and nuclear regions (*third column*), respectively. The fourth column shows cell images by phase contrast microscopy.

Cells removed at 60 min after pheromone release are mainly small-budded, and row *A* shows such a small-budded uninucleate cell with Num1p cortical dots located exclusively in the mother compartment, while phalloidin-stained actin is seen only in the bud and around the bud neck. 15 min later (75 min, row *B*) buds have increased in size, but are still devoid of anti-Num1p staining; actin is concentrated to the bud, but is also seen as cortical dots in the mother cell. Rows *C* and *D* (90 and 105 min, respectively) present mitotic cells with two chromosomal regions and elongated spindles (anti-tubulin fluorescence not shown here). Num1p remains associated mainly with the mother cell periphery, while the cortical actin dots are now evenly distributed between mother and daughter compartment. Row *E* (120 min) shows a large-budded cell with two reorganized nuclei and actin layers concentrated around the bud neck, indicating the stage of cytokinesis. Num1p has reached now a low level, while some weakly stained dots are visible both in mother and daughter compartment. Finally, row *F* (135 min) shows an apparently unbudded cell with a single nuclear region. The asymmetric distribution of cortical actin dots (*second column*) points to the initiation of a new bud, and the few Num1p dots (*first column*) may represent newly synthesized protein of an early S phase cell.

The cell types shown in Fig. 5 represent at least 60% (frequently 90%) of the various populations, indicating a reasonable degree of synchrony. The remaining cells were
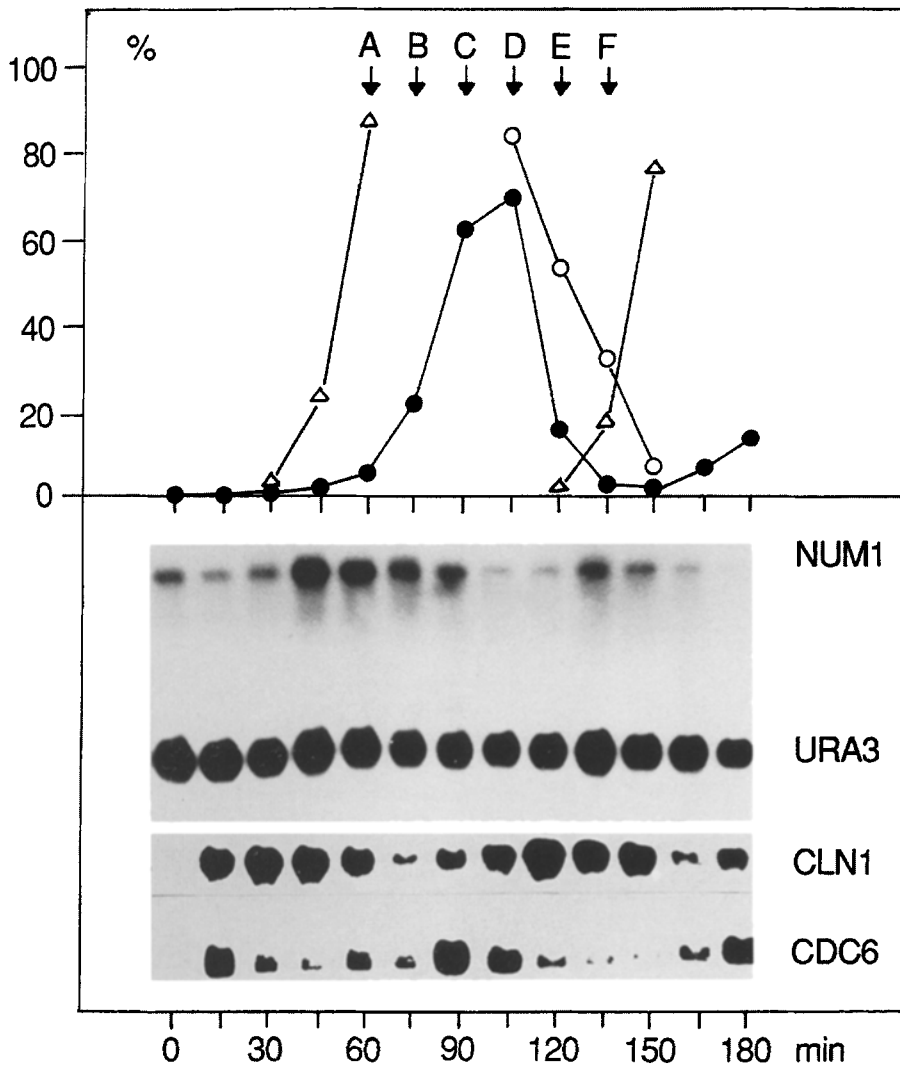
Figure 4. Fluctuation of *NUM1* mRNA in cells synchronized by release from pheromone arrest. Exponentially grown cells of the pheromone-hypersensitive strain RH-270-2B were treated for 1.5 h with α-pheromone. Arrested zygote cells were released at zero time by resuspension in preconditioned pheromone-free medium (Zwerschke et al., 1994), and aliquots were removed at 15-min intervals for cytological determinations, Northern hybridization analysis, and immunofluorescence microscopy. The upper part shows the percentage of small-budded cells (△-△), large-budded cells (○-○), and anaphase cells with an elongated nuclear spindle (●-●). The lower part shows the content of transcripts of *NUM1*, *CLN1*, *CDC6*, and *URA3* in total RNA. The RNA input was controlled by measuring the O.D. at 260 nm, and by staining rRNA bands upon gel electrophoresis. Samples removed at indicated times (*A–F, top*) were used for immunofluorescence analysis (see Fig. 5).

also stained by anti-Num1p, but appeared to be in different stages of the cell cycle. Only 1% of cells were not stained.

The intensity of Num1p-specific immunofluorescence is not necessarily a function of Num1p content, due to a possible epitope masking effect. We have therefore measured the fluctuation of Num1p in pheromone-synchronized cells by Western blot analysis of total lysate protein, as shown in Fig. 6. The cytological determinations of this experiment (data not shown) indicated a somewhat different timing of events as compared with the data of Fig. 4: the maximum of telophase cells was reached ~15 min earlier (at 90 min) than in the previous experiment (at 105 min, see Figs. 4 and 5 *D*). The intensity of the immunoreactive 310-kD band in Fig. 6 suggests a similar fluctuation pattern as revealed by the in situ fluorescence data (Fig. 5): the Num1p level is low in pheromone-arrested cells (zero time) and further decreases before the onset of bud formation (30 min after release). Num1p reappears during S phase (45 min), reaches a maximum at early mitosis (60 and 75 min), and drops to a minimum around the telophase stage at 105 min after release. A low amount of Num1p is seen at a stage shortly after cytokinesis (120 min), possibly produced by early S phase cells.

Morphology of Microtubules in Num1-deficient Strains

Fig. 7 shows some morphological features of microtubules in large-budded *num1* cells (strain FMY2). Cells were grown to early stationary phase, a condition known to increase the number of binucleate mother cells (Revardel and Aigle, 1993), and treated with anti-tubulin and DAPI to visualize microtubules (*left column*) and nuclear regions (*middle column*), respectively. Row *A* shows a uninucleate cell with an abnormally elongated and misoriented bundle of AMTs (which should normally extend into the bud), and a short nuclear spindle which is not oriented along the mother/daughter axis. A misoriented spindle is also seen in cells *B* and *C*, showing two different stages of elongation. Again the two bundles of AMTs are unusually long, and one of them is seen to traverse the daughter compartment. The DAPI-stained cell *C* suggests an early stage of chromosome segregation within the mother compartment. Cell *D* contains a telophase nucleus (two separated chromosomal spots connected by an elongated nuclear spindle), which is correctly orientated along the mother/bud axis while remaining in the mother compartment. The cell contains short mother-oriented AMTs, whereas bud-oriented AMTs appear to be absent. Mitosis of a single
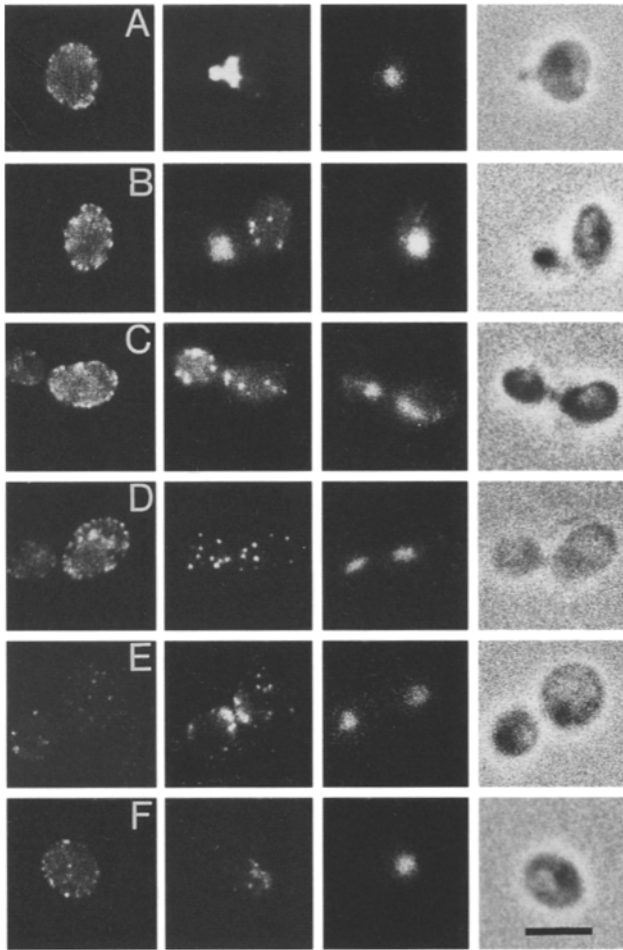
Figure 5. Num1p distribution in RH-270-2B cells synchronized by release from pheromone arrest. Aliquots were removed at 60 min (*A*), 75 min (*B*), 90 min (*C*), 105 min (*D*), 120 min (*E*), and 135 min (*F*) after zero time (see Fig. 4, *top*), and were subsequently treated with anti-Num1p (*first column from left*), rhodamine-conjugated phalloidin (*second column*), and DAPI (*third column*) to stain Num1p, actin and nuclear regions, respectively. The fourth column shows cellular images by phase contrast microscopy. Bar, 10 μm.

mother nucleus seems to be completed in cells *E* and *F*, since the nuclear spindle has apparently collapsed, whereas one or two AMT bundles per reorganized nucleus are still visible.

All cell types shown in Fig. 7 were frequently detected in FMY2 and other *num1* cells grown under similar condi-

tions, and were virtually absent from *NUM1* cells. The data of Table II demonstrate that the percentage of cells with a misoriented spindle increases with the density of cell populations; a similar increase of cells with two chromosomal regions in the mother compartment is observed under the same conditions, confirming earlier findings (Revardel and Aigle, 1993). About 4% of cells contained a misoriented AMT bundle (as seen in Fig. 7 *A*), and this percentage was independent of the cellular density. Such misoriented AMTs were not observed in the isogenic wild-type strain DBY1829. It should also be noted that budding state and nuclear stain of cells showing extended mother-oriented AMTs (as in Fig. 7, *B* and *C*) correspond to the S/G2 period of maximal Num1p expression (see Figs. 4, 5, *B* and *C*, and 6), although the microtubule morphology was not analyzed in synchronized Num1p-deficient cells.

Genetic Interactions of num1 with Mutants Affecting Microtubules

We have replaced one copy of the *NUM1* gene by the marker gene *URA3* in the cold-sensitive *tub1-1/tub1-1* strain FMY60 (see Table I), and the resulting strain FMY61 (relevant genotype *tub1-1/tub1-1 num1-Δ1::URA3/+*) was sporulated and subjected to tetrad analysis, in order to test a possible interaction of the num1 null mutation with the α-tubulin mutation *tub1-1*. All twenty analyzed tetrads produced four viable spores with a 2:2 segregation of the *num1-Δ1::URA3* marker, and all haploid progeny cells were cold-sensitive (growth arrest at 11°C), as expected. However, all *tub1-1,num1* double mutant descendants were also temperature-sensitive (growth arrest at 37°C after performing about eight cell divisions) and grew at a somewhat slower rate at permissive temperature (30°C) than the temperature-resistant *tub1-1,NUM1* descendants. At restrictive temperature, the double mutants accumulate large and osmotically fragile cells, often containing multiple and/or elongated buds, and most cells have lost their viability after 2 d incubation at 37°C.

Possible interactions of the *num1* null mutation with cold-sensitive β-tubulin mutant alleles were tested by *NUM1/URA3* gene replacement in the six homozygous *tub2* diploid strains TH133 to TH138 containing the alleles *tub2-104*, *tub2-401*, *tub2-402*, *tub2-403*, *tub2-404*, and *tub2-405*, respectively. The resulting transformant strains FMY13 to FMY18 were allowed to sporulate, and 40 tetrad asci of each strain were dissected. The strains FMY13 and FMY14 (relevant genotypes *tub2-104/tub2-104 num1-Δ1::URA3/+* and *tub2-401/tub2-401 num1-Δ1::URA3/+*, respectively)
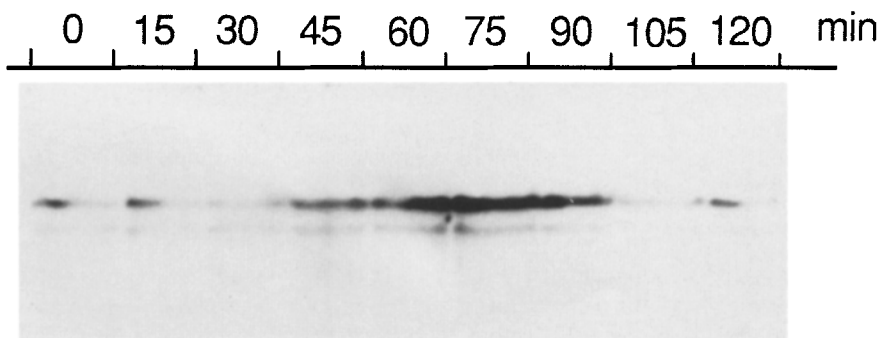

Figure 6. Fluctuation of immunoreactive Num1p in RH-270-2B cells synchronized by release from pheromone arrest. Aliquots were removed at indicated times, and crude lysate protein was subjected to Western blot analysis. For determination of cytological cell cycle markers see legend to Fig. 4.
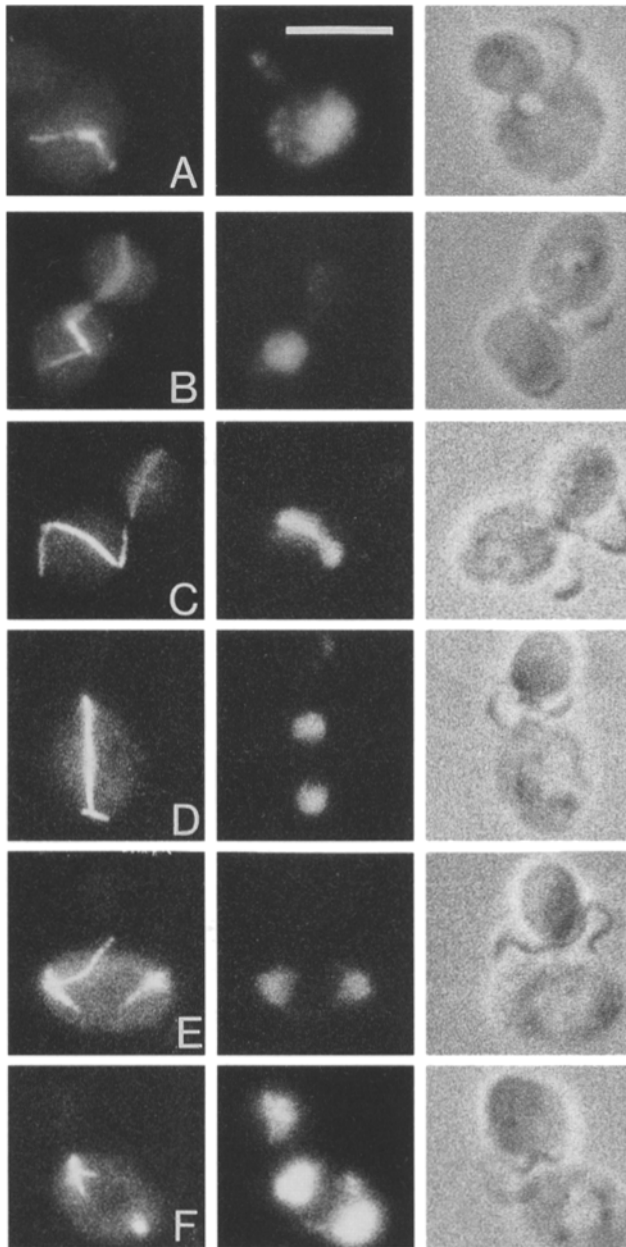
Figure 7. Morphology of microtubules in large-budded *num1-Δ1::URA3* cells. Strain FMY2 was grown to early stationary phase, and cells were subsequently treated with anti-tubulin (*first column from left*) and DAPI (*second column*), to visualize microtubules and nuclear regions, respectively. The third column shows cellular images by phase contrast microscopy. Bar, 10 μm.

produced four viable spores per tetrad with a 2:2 segregation of the *num1-Δ1::URA3* marker. The double mutants *tub2-104,num1* and *tub2-401,num1* did not differ significantly from the corresponding *tub2* single mutants in growth rate and cell morphology. Only two viable spores per tetrad were produced by strains FMY15, FMY16, FMY17, and FMY18 (relevant genotypes: *tub2/tub2* alleles 402 to 405, *num1-Δ1::URA3/+*). All viable spores were uracil-requiring (*NUM1*), and the inviable spores (inferred genotype: *tub2* alleles 402 to 405, *num1-Δ1::URA3*) either did not germinate, or arrested their growth after forming a microcolony of up to 100 cells.

Table II. Nuclear Morphology of *num1-Δ1* Cells (FMY2) Grown to Increasing Densities

Cellular density (OD at 600 nm)	Accumulation of cells	
	With misoriented spindle	With two DNA regions in the mother compartment
	%	
1.8	13	4
4.0	28	20
6.8	37	28

We conclude from these observations that the *num1* null mutation shows synthetic lethality with the cold-sensitive β-tubulin mutant alleles *tub2-402*, *tub2-403*, *tub2-404*, and *tub2-405*, but not with the alleles *tub2-104* and *tub2-401*.
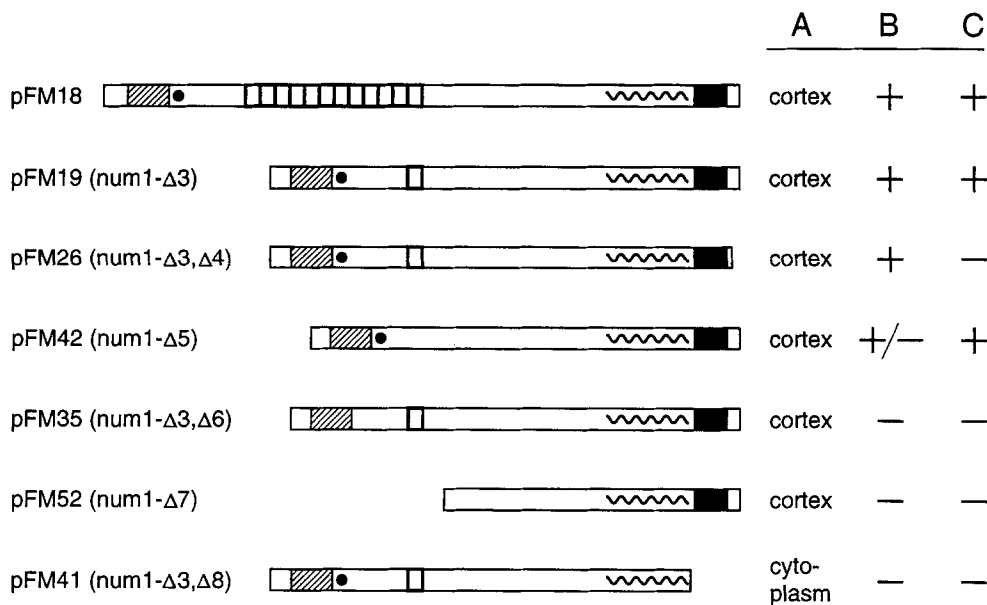
Functional Mapping of NUM1

We have deleted various parts of the *NUM1* gene (see Fig. 1) and introduced the gene variants as centromeric plasmids into *NUM1*-deficient strains, in order to test four functional parameters: (*A*) intracellular localization by indirect immunofluorescence microscopy, (*B*) suppression of the *num1*-specific nuclear migration defect, and (*C*) complementation of the temperature sensitivity of a *tub1-1*, *num1-Δ1* double mutant.

Fig. 8 summarizes the protein maps of the resulting deletion variants together with their functional activities. All tested Num1p variants have retained residues 2182 to 2519, which were used to raise antibodies, and the intensity of indirect immunofluorescence has indicated that all variants are expressed at wild-type levels.

Fig. 9 *A* shows the immunofluorescence pattern of *num1* cells expressing the truncated allele *num1-Δ7* as a GAL4(bd) fusion protein (pFM52); this pattern (cortical dots in the mother cell) is virtually identical to that of *NUM1* cells (Fig. 3 *A*) or *num1* cells containing plasmids pFM18, pFM19, pFM26, pFM42, and pFM35 (data not shown). All Num1p variants encoded by these plasmids have in common their carboxy-terminal PH domain, and the only variant lacking this domain (encoded by pFM41) appears to be released preferentially into the cytoplasm of the mother compartment, as shown in Fig. 9 *B*. These data strongly suggest a cortex-targeting function of the PH domain.

About 30% of large-budded FMY2 cells in cultures approaching stationary phase have two DAPI-stained chromosomal regions in the mother compartment, a morphology reflecting a nuclear migration defect (Kormanec et al., 1991; Revardel and Aigle, 1993). This defect is efficiently suppressed by plasmids pFM18, pFM19, and pFM26, since the content of binucleate mother cells is reduced to weight level (<0.1%). Plasmid pFM42 is partially active (15% binucleate mother cells), and the remaining three plasmids (pFM35, pFM52, and pFM41) are inactive in this assay (28–30% binucleate mother cells). The *tub1-1,num1-Δ1* strain HKY80-2B contains >50% binucleate mother cells, if grown at 30°C to early stationary phase, indicating that the *num1* nuclear migration defect is more pronounced in the presence of the *tub1-1* mutation. The relative suppressing activity of the tested plasmids (see Fig. 8 *B*) was about the same in this strain.

Fig. 10 demonstrates the differential activity of these plas-

		A	B	C
pFM18		cortex	+	+
pFM19 (num1-Δ3)		cortex	+	+
pFM26 (num1-Δ3,Δ4)		cortex	+	−
pFM42 (num1-Δ5)		cortex	+/−	+
pFM35 (num1-Δ3,Δ6)		cortex	−	−
pFM52 (num1-Δ7)		cortex	−	−
pFM41 (num1-Δ3,Δ8)		cyto-plasm	−	−

Figure 8. Functional mapping of Num1p. Features of the Num1p map (*upper line*) are explained in the legend to Fig. 1. Plasmids indicated at left were introduced into the *NUM1*-deficient strain FMY2, and the resulting transformants were analyzed by (*A*) indirect immunofluorescence microscopy, and (*B*) by determining the percentage of large-budded cells with two DAPI-stained regions in the mother, after growth to early stationary phase. Strains containing actively suppressing plasmids (+) produce less than 1% binucleate mother cells, and strains with inactive pla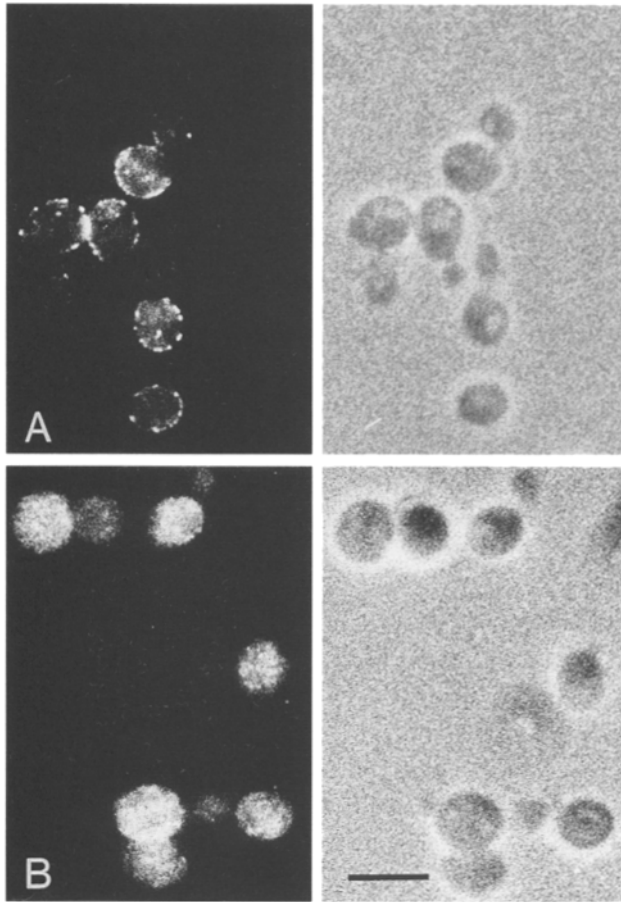smids (−) produce about the same percentage (28–30%) as plasmid-less strain FMY2. FMY2 containing pFM42 produces 15% binucleate mother cells (+/−). (*C*) Plasmids were introduced into the *tub1-1,num1-Δ1* strain HKY80-2B in order to test a complementation of temperature sensitivity (+, growth at 37°; −, arrest at 37°).

mids in complementing the temperature sensitivity of the *tub1-1,num1-Δ1* strain HKY80-B2. Two plasmids (pFM18 and pFM19) are active, and three plasmids are inactive in both assays (see lanes *B* and *C* of Fig. 8), whereas plasmids pFM26 and pFM42 behave differently in the two assays: pFM26 suppresses the nuclear migration defect of *TUB1*, *num1* cells, but does not complement the temperature sensitivity of *tub1-1,num1* cells, and pFM42 has only a partial effect in suppressing the nuclear migration defect, but is fully active in complementing the *tub1-1,num1-Δ1* temperature sensitivity.

Discussion

Previous observations have indicated a role of the *NUM1* gene product in the control of nuclear migration at the G2 phase of the cell cycle (Kormanec et al., 1991). Here we demonstrate a temporal and spatial control of *NUM1* gene expression: the *NUM1* transcript transiently accumulates at the S/G2 phase of cells synchronized by two different methods, and the Num1 protein associates at the same period of the cell cycle to the cortex of mother cells, where it remains located mainly up to the stage of cytokinesis. Thus, *NUM1* belongs to the class of periodically expressed genes encoding stage-specific cyclins, histones, transcriptional regulators, and proteins involved in DNA synthesis (for a recent review see Küntzel et al., 1994).

The *NUM1* mRNA fluctuation pattern resembles that of histones (Osley, 1991) and of the mitotic cyclins *CLB3* and *CLB4* (Richardson et al., 1992). The latter two stage-specific activators of the *CDC28* protein kinase are required for the assembly of a short nuclear spindle in pre-anaphase cells (Richardson et al., 1992; Schwob and Nasmyth, 1993).

The *NUM1* gene maps close to the dihydrolipoyl trans-succinylase gene *KGD2* (Repetto and Tzagoloff, 1990), and both genes share a 561-bp promoter region controlling a divergent transcription of opposite DNA strands (see Fig. 1). However, both genes appear to be differentially regulated: *KGD2* transcription is glucose-repressible (Repetto and Tzagoloff, 1990) and constant throughout the cell cycle, whereas the periodic *NUM1* transcription is enhanced in cells grown in glucose media (our unpublished data).

Indirect immunofluorescence microscopy of *NUM1* cells treated with anti-Num1p has visualized the Num1p antigen as cortical dots located at the periphery of mother cells, while the bud region is not stained by antibody. This asymmetrical distribution pattern is opposed to that of cortical actin patches which concentrate around the bud neck and within small buds during the S/G2 stage of the cell cycle (for review see Welch et al., 1994). The cellular content of Num1p cortical dots decreases at the cytokinesis stage of the cell cycle and increases again when small buds are visible. Western blot analysis of pheromone-synchronized cells has also shown a pronounced fluctuation of Num1p during the cell cycle.

Our functional mapping data suggest that the carboxy-terminal PH domain of Num1p serves as a "cortex-targeting" signal: all tested Nump1 variants containing the PH domain associate with the mother cell cortex, even after deleting functionally important regions, and only the removal of the PH domain leads to a cytosolic localization of Num1p. PH domains are found in cytoskeletal proteins like spectrin, pleckstrin, and dynamin, but also in many proteins involved in signal transduction, such as GTPase-activating proteins, protein kinases, and phospholipases (Musacchio et al., 1993; Gibson et al., 1994). Interestingly, a Num1p region including the PH domain (residues 2301 to 2742) shows significant sequence similarity with a corresponding region of the *Aspergillus nidulans ApsA* protein, which is required for nuclear positioning and entry of nuclei into primary buds (sterigmata) during the development of conidiophores (Fischer and Timberlake, 1995). The similarity between Num1p and ApsAp is most pronounced within the PH domain, whereas other common

Figure 9. Immunolocalization of truncated Num1p derivatives encoded by alleles *num1-Δ7* (*A*, strain FMY2-52) and *num1-Δ3,Δ8* (*B*, strain FMY2-41). (*Left column*) Indirect immunofluorescence of cells treated with anti-Num1p antibodies. (*Right column*) Phase contrast microscopy.

features of both proteins (an NH₂-terminal coiled-coil domain and central tandem repeats) are not conserved in their primary structure.

A common function of PH domains could be the recognition of phosphorylated serine/threonine residues in specific peptides (Gibson et al., 1994) and/or the interaction with the membrane lipid phosphatidyl-inositol-4,5-bisphosphate (Harlan et al., 1994). The latter function would imply a direct association of Num1p with lipids of the mother cell membrane; alternatively, Num1p could be anchored via its PH domain to proteins associated with the plasma membrane of mother cells.

Several observations suggest that Num1p affects microtubular functions: (*a*) *NUM1*-deficient strains accumulate large-budded cells with a misoriented nuclear spindle and elongated AMTs, a phenotype characteristic of conditional-lethal β-tubulin and actin mutants (Huffaker et al., 1988; Palmer et al., 1992), as well as of null mutants lacking either the dynein heavy chain Dhc1p/Dyn1p (Li et al., 1993; Eshel et al., 1993), the centractin homolog Act3p/Act5p (Muhua et al., 1994; Clark and Meyer, 1994), or the dynein-associated protein Jnm1p (McMillan and Tatchell, 1994). (*b*) The AMTs of *num1* cells are sometimes misoriented and do not extend into the bud (see Fig. 7 *A*). This is

in contrast to *jnm1* mutant cells, where bud-oriented AMTs always appear to extend to the mother/bud neck (McMillan and Tatchell, 1994). (*c*) Misoriented nuclei tend to perform mitosis and nuclear division in the mother compartment of large-budded *num1* cells (see Fig. 7) leading to the accumulation of "binucleate mother cells" (Kormanec et al., 1991; Revardel and Aigle, 1993). Again, this behavior is seen in many other mutants affecting microtubular functions, and it confirms that the mitotic functions of the nuclear spindle are not affected by mutations impairing AMTs (Sullivan and Huffaker, 1992). (*d*) The deletion of the nonessential *NUM1* gene has synthetic effects in the cold-sensitive α-tubulin mutant *tub1-1* (Stearns and Botstein, 1988) and in certain cold-sensitive β-tubulin (*tub2*) mutant alleles (Huffaker et al., 1988). The *num1-Δ1* null mutation confers conditional lethality at 37°C to *tub1-1* strains, and is lethal at all temperatures in combination with the alleles *tub2-402*, *tub2-403*, *tub2-404*, and *tub2-405*. The four *tub2* mutations interacting with *num1-Δ1* · are clustered within a COOH-terminal β-tubulin domain (residues 375-424), while the noninteracting allele *tub2-401* maps more upstream at residues 233-245 (Huffaker et al., 1988).

The four *num1*-interacting *tub2* alleles have quite different effects on the content of nuclear and astral microtubules at restrictive temperature: two mutant alleles (*tub2-403* and *tub2-405*) contain greatly diminished levels of both kinds of microtubules, one allele (*tub2-402*) contains predominantly astral microtubules, and allele *tub2-404* contains prominent nuclear and astral microtubule arrays; the two noninteracting alleles contain predominantly nuclear microtubules (*tub2-104*) or apparently lack both kinds of microtubules (*tub2-401*) (Huffaker et al., 1988).

It is difficult to deduce from these data a common property distinguishing *num1*-interacting from noninteracting *tub2* alleles; perhaps the ability to produce AMTs is critical for lethal interaction with *num1-Δ1*.

The most prominent structural feature of Num1p is a 12-fold near-perfect repetition of a peptide of 64 residues (Kormanec et al., 1991). However, our deletion experiments suggest that the amplification of this peptide is not critical for function, since a single repeat unit is sufficient to suppress the nuclear migration defect in *TUB1,num1* cells as well as the temperature sensitivity of *tub1-1,num1* mutants. A similar conclusion can be drawn from the observed polymorphism of the repetitive region in different yeast wild-type strains (Revardel and Aigle, 1993).

The deletion of the remaining single repeat unit in allele *num1-Δ5* reduces the ability to suppress the nuclear migration defect in *TUB1,num1* cells, but surprisingly does not affect the rescue of conditional lethality of the *tub1-1,num1* double mutation. The opposite effect is observed if the last 30 residues of Num1p are removed, which include a cluster of potential phosphorylation sites of cAMP-dependent protein kinase and protein kinase C (Kormanec et al., 1991): this deletion abolishes the ability to rescue the temperature sensitivity of *tub1-1,num1* double mutants, but does not affect the suppression of the nuclear migration defect in *TUB1,num1* cells. Both activities are lost by deleting a potential EF-hand Ca²⁺-binding site (Δ6) or a carboxy-terminal region including the PH domain (Δ8).
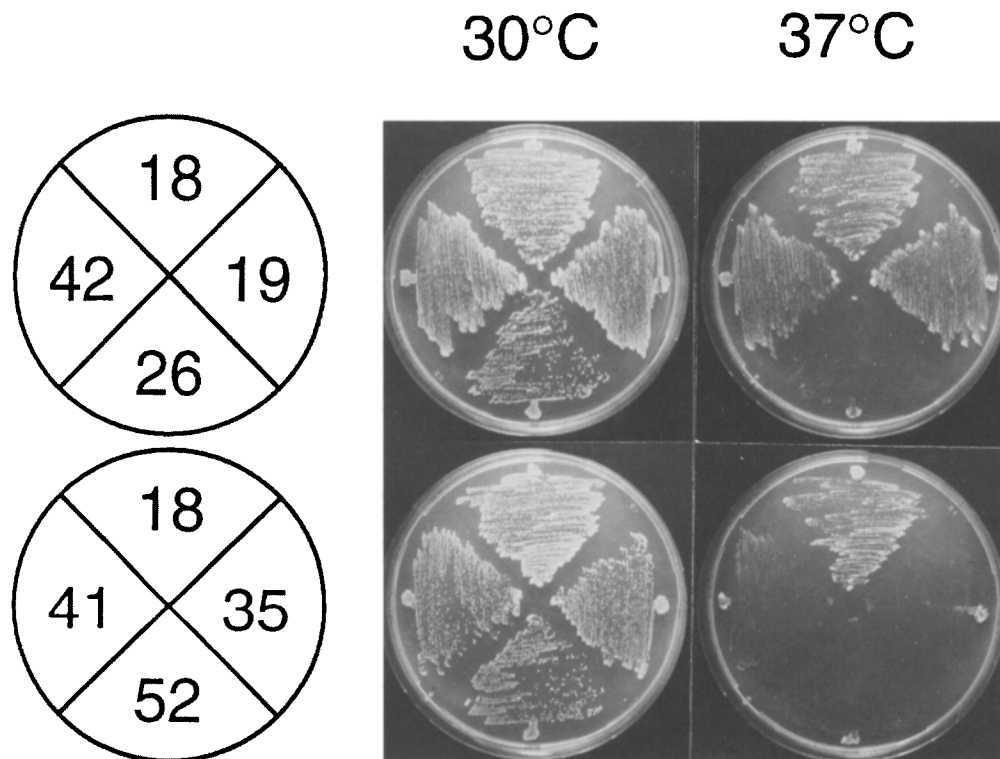
Figure 10. Complementation of *tub1-1,num1-Δ1* temperature sensitivity (strain HKY80-2B) by plasmids containing intact and deleted *NUM1* variants. Strains and relevant genotypes: 18, *tub1-1 num1-Δ1* pFM18 (NUM1); 19, *tub1-1 num1-Δ1* pFM19 (num1-Δ3); 26, *tub1-1 num1-Δ1* pFM26 (*num1-Δ3,Δ4*); 42, *tub1-1 num1-Δ1* pFM42 (num1-Δ5); 35, *tub1-1 num1-Δ1* pFM35 (num1-Δ3,Δ6); 52, *tub1-1 num1-Δ1* pFM52 (num1-Δ7); 41, *tub1-1 num1-Δ1* pFMY41 (num1-Δ3,Δ8). Cells were incubated for 2 d on selective medium at 30°C and 37°C.

These observations point to differential roles of Num1p in controlling AMT functions and/or nuclear migration. However, the specific association of Num1p with the mother cell cortex is difficult to reconcile with effects on mother-distal AMTs, which are sometimes not properly oriented towards the bud; furthermore, both mother-distal and mother-proximal AMTs are often abnormally elongated in *num1* cells. A similar problem concerns the role of Jnm1p, a protein located in the bud or near the bud-oriented SPB. This protein affects not only bud-oriented, but also mother-oriented AMTs, which both appear to be abnormally elongated in *JNM1*-deficient strains (McMillan and Tatchell, 1994).

The first evidence for a functional orientation of SPBs (via their AMTs) toward the cortex of mother and bud compartment was provided by the observation that the old SPB remains in the mother cell, whereas the new SPB (formed by SPB duplication) segregates into the daughter cell (Vallen et al., 1992).

A more recent model of nuclear migration in budding yeast has postulated the positioning of the pre-anaphase nucleus by transiently tethering AMTs to cortical sites at the mother compartment and at the bud or bud/mother neck region (Schroer, 1994). Candidates for tethering bud-oriented AMTs are components of the dynein/dynactin complex encoded by *DHC1/DYN1*, *ACT3/ACT5*, and *JNM1* (Schroer, 1994; Macmillan and Tatchell, 1994), whereas Num1p is a possible candidate for tethering AMTs to the mother cortex during its transient expression period at S/G2 phase. The failure to attach either mother- or bud-oriented AMTs to their respective cortical sites (e.g., by deleting *NUM1*, *DHC1/DYN1*, *ACT3/ACT5*, or *JNM1*) could possibly lead to the release from both attachment sites, followed by the abnormal elongation of both kinds of AMTs.

Alternatively, Num1p may control AMT functions more indirectly, e.g., by acting in a signaling pathway involved in the structural modification of microtubules or microtubule-associated proteins. Indeed, some functionally important elements of Num1p (a potential EF hand Ca^{2+}-binding site, a PH domain frequently found in signaling proteins, and clusters of potential phosphorylation sites for cAMP-dependent protein kinase and/or protein kinase C) point to a role of this mother-specific protein in signal transduction.

References

Burnette, W. N. 1981. "Western blotting": electrophoretic transfer of proteins from sodium dodecyl sulfate-polyacrylamide gels to unmodified nitrocellulose and autoradiographic detection with antibody and radioiodinated protein A. *Anal. Biochem.* 112:195–203.

Byers, B., and L. Goetsch. 1975. Behavior of spindles and spindle plaques in the cell cycle and conjugation of *Saccharomyces cerevisiae. J. Bacteriol.* 124:511–523.

Clark, S. W., and D. I. Meyer. 1994. *ACT3*: a putative centractin homologue in *S. cerevisiae* is required for proper orientation of the mitotic spindle. *J. Cell Biol.* 127:129–138.

Eshel, D., L. A. Urrestarazu, S. Vissers, J.-C. Jauniaux, J. C. van Vliet-Reedijk, R. J. Planta, and I. R. Gibbons. 1993. Cyto-plasmic dynein is required for normal nuclear segregation in yeast. *Proc. Natl. Acad. Sci. USA.* 90:11172–11176.

Fischer, R., and W. E. Timberlake. 1995. *Aspergillus nidulans apsA* (Anucleate Primary Sterigmata) encodes a coiled-coil protein required for nuclear positioning and completion of asexual development. *J. Cell Biol.* 128:485–498.

Gibson, T. J., M. Hyvönen, E. Birney, A. Musacchio, and M. Saraste. 1994. PH domain: the first anniversary. *Trends Biochem. Sci.* 19:349–353.

Harlan, J. E., P. J. Hajduk, H. S. Yoon, and S. W. Fesik. 1994. Pleckstrin homology domains bind to phosphatidylinositol-4,5-bisphosphate. *Nature (Lond.).* 371:168–170.

Huffaker, T. C., J. H. Thomas, and D. Botstein. 1988. Diverse effects of β-tubulin mutations on microtubule formation and function. *J. Cell Biol.* 106:1997–2010.

Jacobs, C. W., A. E. M. Adams, P. J. Szaniszlo, and J. R. Pringle. 1988. Functions of microtubules in the *Saccharomyces cerevisiae* cell cycle. *J. Cell Biol.* 107:1409–1426.

Kilmartin, J. V., and A. E. M. Adams. 1984. Structural rearrangements of tubulin and actin during the cell cycle of the yeast *Saccharomyces. J. Cell Biol.* 98:922–933.

Kormanec, J., I. Schaaf-Gerstenschläger, F. K. Zimmermann, D. Perecko, and H. Küntzel. 1991. Nuclear migration in *Saccharomyces cerevisiae* is controlled by the highly repetitive 313 kDa *NUM1* protein. *Mol. Gen. Genet.* 230:277–287.

Küntzel, H., H.-W. Rottjakob, A. Schwed, and W. Zwerschke. 1994. START control in cycling *Saccharomyces cerevisiae* cells. *Progr. Nucleic Acid Res. Mol. Biol.* 48:1–28.

Li, Y.-Y., E. Yeh, T. Hays, and K. Bloom. 1993. Disruption of mitotic spindle orientation in a yeast dynein mutant. *Proc. Natl. Acad. Sci. USA.* 90:10096–10100.

Lupas, A., M. Van Dyke, and J. Stock. 1991. Predicting coiled coils from protein sequences. *Science (Wash. DC).* 252:1162–1164.

McMillan, J. N., and K. Tatchell. 1994. The *JNM1* gene in the yeast *Saccharomyces cerevisiae* is required for nuclear migration and spindle orientation during the mitotic cell cycle. *J. Cell Biol.* 125:143–158.

Muhua, L., T. S. Karpova, and J. A. Cooper. 1994. A yeast actin-related protein homologous to that in vertebrate dynactin complex is important for spindle orientation and nuclear migration. *Cell.* 78:669–679.

Munder, T., M. Mink, and H. Küntzel. 1988. Domains of the *Saccharomyces cerevisiae CDC25* gene controlling mitosis and meiosis. *Mol. Gen. Genet.* 214:271–277.

Musacchio, A., T. Gibson, P. Rice, J. Thompson, and M. Saraste. 1993. The PH domain: a common piece in the structural patchwork of signalling proteins. *Trends Biochem. Sci.* 18:343–348.

Osley, M. A. 1991. The regulation of histone synthesis in the cell cycle. *Annu. Rev. Biochem.* 60:827–861.

Palmer, R. E., D. S. Sullivan, T. Huffaker, and D. Koshland. 1992. Role of astral microtubules and actin in spindle orientation and migration in the budding yeast, *Saccharomyces cerevisiae. J. Cell Biol.* 119:583–593.

Pringle, J. R., and L. H. Hartwell. 1981. The *Saccharomyces cerevisiae* cell cycle. *In* The Molecular Biology of the Yeast Saccharomyces. Life Cycle and Inheritance. Strathern, J. N., E. W. Jones, and J. R. Broach, editors. Cold Spring Harbor Laboratory, Cold Spring Harbor, NY. 97–142.

Pringle, J. R., A. E. M. Adams, D. G. Drubin, and B. K. Haarer. 1991. Immuno-

fluorescence methods for yeast. *Methods Enzymol.* 194:565–602.

Repetto, B., and A. Tzagoloff. 1990. Structure and regulation of *KGD2*, the structural gene for yeast dihydrolipoyl trans-succinylase. *Mol. Cell. Biol.* 10:4221–4232.

Revardel, E., and M. Aigle. 1993. The *NUM1* yeast gene: length polymorphism and physiological aspects of mutant phenotype. *Yeast.* 9:495–506.

Richardson, H., D. J. Lew, M. Henze, K. Sugimoto, and S. I. Reed. 1992. Cyclin-B homologs in *Saccharomyces cerevisiae* function in S phase and in G2. *Genes Dev.* 6:2021–2034.

Rothstein, R. J. 1983. One-step gene disruption in yeast. *Methods Enzymol.* 101:202–210.

Sambrook, J., E. F. Fritsch, and T. Maniatis. 1989. Molecular Cloning: A Laboratory Manual. Cold Spring Harbor Laboratory Press, Cold Spring Harbor, NY.

Schatz, P. J., F. Solomon, and D. Botstein. 1986. Genetically essential and nonessential α-tubulin genes specify functionally interchangeable proteins. *Mol. Cell. Biol.* 6:3722–3733.

Schroer, T. A. 1994. New insights into the interaction of cytoplasmic dynein with the actin-related protein, Arp1. *J. Cell Biol.* 127:1–4.

Schwob, E., and K. Nasmyth. 1993. *CLB5* and *CLB6*, a new pair of B cyclins involved in DNA replication in *Saccharomyces cerevisiae. Genes Dev.* 7:1160–1175.

Smith, D. E., and P. A. Fisher. 1984. Identification, developmental regulation, and response to heat shock of two antigenically related forms of a major nuclear envelope protein in Drosophila embryos: application of an improved method for affinity purification of antibodies using polypeptides immobilized on nitrocellulose blots. *J. Cell Biol.* 99:20–28.

Smith, D. B., and K. S. Johnson. 1988. Single-step purification of polypeptides expressed in *Escherichia coli* as fusions with glutathione-S-transferase. *Gene (Amst.).* 67:31–40.

Stearns, T., and D. Botstein. 1988. Unlinked noncomplementation: isolation of new conditional-lethal mutations in each of the tubulin genes of *Saccharomyces cerevisiae. Genetics.* 119:249–260.

Sullivan, D. S., and T. C. Huffaker. 1992. Astral microtubules are not required for anaphase B in *Saccharomyces cerevisiae. J. Cell Biol.* 119:379–388.

Vallen, E. A., T. Y. Scherson, T. Roberts, K. van Zee, and M. D. Rose. 1992. Asymmetric mitotic segregation of the yeast spindle pole body. *Cell.* 69:505–515.

Welch, M. D., D. A. Holtzman, and D. G. Drubin. 1994. The yeast actin cytoskeleton. *Curr. Opin. Cell Biol.* 6:110–119.

Zwerschke, W., H.-W. Rottjakob, and H. Küntzel. 1994. The *Saccharomyces cerevisiae CDC6* gene is transcribed at late mitosis and encodes a ATP/GTPase controlling S phase initiation. *J. Biol. Chem.* 269:23351–23356.